HT2020-10838

ASSESSMENT OF MODELS FOR EXTRACTING THERMAL CONDUCTIVITY FROM FREQUENCY DOMAIN THERMOREFLECTANCE EXPERIMENTS

SIDDHARTH SAURAV and SANDIP MAZUMDER*

Department of Mechanical and Aerospace Engineering The Ohio State University, Columbus, OH 43210, USA

ABSTRACT

The Fourier heat conduction and the hyperbolic heat conduction equations were solved numerically to simulate a frequencydomain thermoreflectance (FDTR) experimental setup. Numerical solutions enable use of realistic boundary conditions, such as convective cooling from the various surfaces of the substrate and transducer. The equations were solved in time domain and the phase lag between the temperature at the center of the transducer and the modulated pump laser signal were computed for a modulation frequency range of 200 kHz to 200 MHz. It was found that the numerical predictions fit the experimentally measured phase lag better than analytical frequency-domain solutions of the Fourier heat equation based on Hankel transforms. The effects of boundary conditions were investigated and it was found that if the substrate (computational domain) is sufficiently large, the far-field boundary conditions have no effect on the computed phase lag. The interface conductance between the transducer and the substrate was also treated as a parameter, and was found to have some effect on the predicted thermal conductivity, but only in certain regimes. The hyperbolic heat conduction equation yielded identical results as the Fourier heat conduction equation for the particular case studied. The thermal conductivity value (best fit) for the silicon substrate considered in this study was found to be 108 W/m/K, which is slightly different from previously reported values for the same experimental data.

INTRODUCTION

The ability to control and manipulate heat transport at the nanoscale is important for the advancement of thermal management strategies in electronic and optoelectronic devices. In the past decade, noncontact optical pump probe techniques based on thermoreflectance have been used extensively for the study of heat transport at very small time and length scales. The two most commonly used techniques are the Time Domain Thermo-Reflectance (TDTR) technique and the Frequency Domain Thermo-Reflectance (FDTR) technique. In TDTR, the

sample is heated using a pulsed laser that is modulated, and the surface is probed using a time-delayed laser that measures the change in the reflectivity of the surface caused by the change in temperature of the sample [1-3]. In FDTR, the sample is, instead, heated using a modulated continuous wave pump laser beam resulting in surface temperature (reflectivity) oscillations, which are then monitored using a probe laser. The lag in phase between the pump and probe laser signals is recorded. In either method, the surface of the target material (whose thermal properties are sought) is covered with an ultrathin metallic layer, often referred to as the *transducer*.

Extraction of the thermal conductivity of the substrate from measured thermoreflectance data requires use of a thermal transport model. Since both TDTR and FDTR experiments measure surface temperature (or some indicator of it), while thermal conductivity is a volumetric property, the two quantities can only be related though a thermal transport model. Furthermore, the presence of the transducer complicates matters, since the heat must now transfer through multiple layers and the imperfect contact between the two layers. The most common model used for this purpose is based on the solution of the Fourier heat conduction equation in frequency domain. This was brought to the limelight by Cahill [1]. Multiple layers are treated using the well-known Feldman algorithm [4]. Interfaces between layers are treated as artificial layers whose thermal properties are adjusted to reproduce measured interface conductance values.

The thermal conductivity extracted from FDTR experiments using such a Fourier law based model has been found to change when the modulation frequency of the pump laser is changed [1-3,5]. This behavior is attributed to the fact that when the laser modulation frequency is high, the thermal penetration depth, which is inversely proportional to the square root of the modulation frequency, is small, and can often be smaller than the mean free path of some phonons. As a result, some phonons hardly scatter. This results is so-called ballistic-diffusive transport or quasi-ballistic transport. In this regime of transport, the effective thermal conductivity has been found to be smaller

than the bulk value—a phenomenon known as *thermal* conductivity suppression [5-7].

In an effort to capture ballistic effects and develop a model that can predict thermal conductivity suppression across all modulation frequencies, researchers have proposed various enhancements to Fourier law based models. One class of these models make use of the hyperbolic heat conduction equation, which accounts for finite group velocity of the phonons. The Cattaneo equation, the Cattaneo-Vernotte model, and the dual phase lag model fall in this category [8,9]. Even though the hyperbolic heat conduction equation accommodates finite phonon speed, all phonons, regardless of their type and frequency, are assumed to have the same speed. In an effort to remove this deficiency, Ramu and Bowers [10] proposed a twoband model in which a cut-off frequency is used to classify the phonons into ballistic and diffusive phonons. The ballistic phonons are then treated by adding a higher order correction term to the Fourier law that is derived from the Boltzmann Transport Equation (BTE) for phonons. In a similar model, Ma [11] treated non-diffusive effects by introducing an additional term in the Fourier heat conduction equation that involves the characteristic ballistic heat transport length as an additional parameter to the thermal conductivity of the substrate. This characteristic length is an additional tuning parameter in this model. In the ballisticdiffusive model proposed by Chen [12], and later expanded to complex three-dimensional geometry by Mittal and Mazumder [13,14], the phonon intensity is split into a diffusive component and a ballistic component. The diffusive component, by virtue of being more or less isotropic, can be treated using the method of spherical harmonics, while the ballistic component is treated using a surface-to-surface exchange formulation.

principle, the multidimensional phonon encapsulates the necessary phonon physics, and should be used as the model to interpret the measured data, as demonstrated by Ali and Mazumder [15] for TDTR experiments. All of the aforementioned approximate models were proposed and exercised to avoid full-fledged (and very time-consuming) solution to the phonon BTE, and continue to be used for the extraction of thermal conductivity from both TDTR and FDTR experimental data. Further, the equations used for this purpose (to be presented in the next section), employ transform methods in frequency domain that require certain assumptions. In this work, we re-assess the efficacy of such models by solving the governing heat conduction equations numerically in time domain. This allows us to assess the validity of some of the assumptions invoked in transform methods. Specifically, the objective is to answer the following questions: (1) what is the effect of heat loss from the system? (2) what is the effect of the finite thickness of the substrate? (3) what is the effect of the interface conductance between the substrate and the transducer? In addition to the Fourier heat conduction equation, the hyperbolic heat conduction equation is also explored in an effort to capture quasi-ballistic effects.

THEORY AND SOLUTION METHOD

Anaytical Solution: Fourier Heat Conduction

The analytical solution to the Fourier heat conduction equation with periodic heat flux boundary conditions is obtained by first transforming the original equation in time domain to an equation in frequency domain, followed by invoking a Fourier transform. Details of this procedure are provided elsewhere [16]. In this case, the frequency domain solution for a single layer is obtained by taking the Hankel transform of the response due to the laser beam since the sample is assumed to have cylindrical symmetry. For a semi-infinite solid being heated by a periodic heat flux operating at an angular frequency ω , the response of the surface is given by [16,1],

$$\Delta T = 2\pi A \int_{0}^{\infty} G(p) \exp[-\pi^{2} p^{2} (w_{0}^{2} + w_{1}^{2})/2] p \, dp \,, \tag{1}$$

where p is the Hankel transform parameter, w_0 and w_1 are the $1/e^2$ radius of the pump and the probe beam, respectively, and A is the amplitude factor of the heat flux (due to the pump laser). The quantity ΔT denotes the weighted (over the radius of the probe laser beam) average temperature and has both a real and an imaginary part. The quantity, G(p), in Eq. (1) is given by

$$G(p) = \frac{1}{k\sqrt{4\pi^2 p^2 + q^2}}; \ q^2 = \frac{i\omega}{\alpha},\tag{2}$$

where k is the thermal conductivity of the solid (or substrate) and α its thermal diffusivity.

When the solution is extended to a layered structure using the Feldman algorithm [4], as proposed in [1], the layers are numbered starting from n=1 being the one closest to the surface being heated by the laser. The thickness, thermal conductivity, and thermal diffusivity of each layer are denoted by L_n , k_n , and α_n , respectively. The expression for G(k), shown in Eq. (2), is then replaced by

$$G(p) = \frac{1}{\gamma_1} \left(\frac{B_1^+ - B_1^-}{B_1^+ + B_1^-} \right); \ \gamma_n = k_n u_n; \ u_n = \sqrt{4\pi^2 p^2 + q_n^2} \ . \tag{3}$$

The quantities B^+ and B^- are the growth and decay exponents along the thickness. For an N-layered structure, the furthest layer only has decay ($B_N^-=1$) and has no growth ($B_N^+=0$). The growth and decay exponents for the other layers are determined using the following recursive relation starting from the N-th layer:

$$\begin{pmatrix}
B_n^+ \\
B_n^-
\end{pmatrix} = \frac{1}{2\gamma_n} \begin{bmatrix} \exp(-u_n L_n) & 0 \\
0 & \exp(u_n L_n) \end{bmatrix} \times \begin{bmatrix} \gamma_n + \gamma_{n+1} & \gamma_n - \gamma_{n+1} \\ \gamma_n - \gamma_{n+1} & \gamma_n + \gamma_{n+1} \end{bmatrix} \begin{bmatrix} B_{n+1}^+ \\ B_{n+1}^- \end{bmatrix} .$$
(4)

In this method, the interface between layers is treated as an artificial layer for which the thermal conductivity, thermal diffusivity and thickness are chosen such that a known thermal conductance value (= k_n / L_n) is matched, and the thermal mass is small. However, lateral (radial) conduction within the interface, which is unphysical, cannot be eliminated.

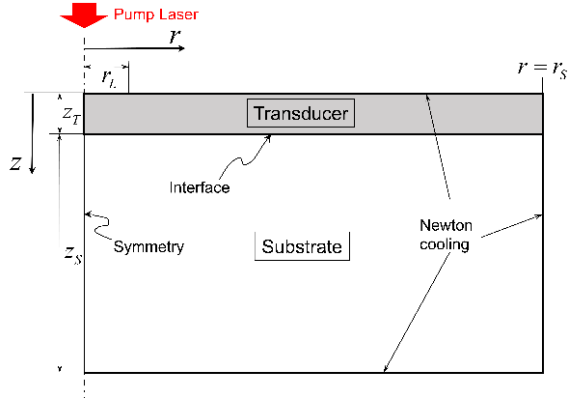


Figure 1: Schematic of the computational domain and boundary conditions.

Numerical Solution: Fourier Heat Conduction

The starting point of the numerical solution is the transient Fourier heat conduction equation. Under the axisymmetric assumption, and constant thermophysical properties, this equation may be written in cylindrical coordinates as [16]

$$\rho c \frac{\partial T}{\partial t} = k \nabla^2 T = k \frac{\partial^2 T}{\partial z^2} + \frac{k}{r} \frac{\partial}{\partial r} \left(r \frac{\partial T}{\partial r} \right). \tag{5}$$

where z is in the through-plane direction, and r is in the radial or in-plane direction, as shown in Fig. 1. The boundary conditions in the section where the laser is shining ($r \le r_L$) is written as

$$k \frac{\partial T}{\partial z} \Big|_{(t,0,r \le r_t)} = q_L''(r)[1 + \sin \omega t], \qquad (6a)$$

where $q_L''(r)$ is the radially varying laser heat flux profile, and is assumed to be Gaussian in shape [1]. As noted in Eq. (6), the laser flux also has a temporally varying component with modulation frequency ω . At the axis of symmetry, the boundary condition is written as

$$\left. \frac{\partial T}{\partial r} \right|_{(t,z,0)} = 0 \ . \tag{6b}$$

On the top surface outside of the laser spot and the external (side and bottom) surfaces of the substrate, a Newton cooling boundary condition was used, namely

Top surface:
$$-k \frac{\partial T}{\partial z}\Big|_{(t,0,r>r_L)} = h_t \left[T(t,0,r>r_L) - T_\infty\right],$$
 (6c)

Side surface:
$$-k \frac{\partial T}{\partial r}\Big|_{(t,z,r_s)} = h_s [T(t,z,r_s) - T_\infty],$$
 (6d)

Bottom surface:
$$k \frac{\partial T}{\partial z}\Big|_{(t,z_T+z_S,r)} = h_b \left[T(t,z_T+z_S,r) - T_\infty \right],$$
 (6e)

where h_t , h_s , and h_b are the heat transfer coefficients on the top, side, and bottom surfaces, respectively, and T_{∞} is the ambient temperature.

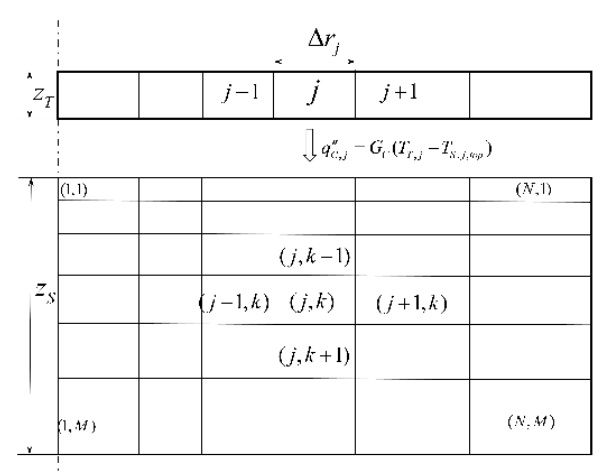


Figure 2: Schematic representation of the stretched mesh used for computations in the two different regions and their coupling.

For numerical solution of Eq. (5) subject to the boundary conditions in Eq. (6), the solution domain is first split into two regions: the transducer and the substrate. The transducer is very thin, and consequently, may be assumed to have negligible temperature gradient in the axial or z-direction. Thus, it may be split into a series of radial control volumes, as shown in Fig. 2. Applying the finite-volume procedure [17] to these control volumes, we obtain

$$\left[\frac{k_{T}z_{T}(2r_{j} + \Delta r_{j})}{\Delta r_{j} + \Delta r_{j+1}} + \frac{k_{T}z_{T}(2r_{j} - \Delta r_{j})}{\Delta r_{j} + \Delta r_{j-1}} + \rho_{T}c_{T}z_{T} \frac{2r_{j}\Delta r_{j}}{\Delta t}\right] T_{T,j}
- \left[\frac{k_{T}z_{T}(2r_{j} + \Delta r_{j})}{\Delta r_{j} + \Delta r_{j+1}}\right] T_{T,j+1} - \left[\frac{k_{T}z_{T}(2r_{j} - \Delta r_{j})}{\Delta r_{j} + \Delta r_{j-1}}\right] T_{T,j-1}, \quad (7)$$

$$= \rho_{T}c_{T}z_{T} \frac{2r_{j}\Delta r_{j}}{\Delta t} T_{T,j}^{old} + 2q_{t,j}'' r_{j}\Delta r_{j} - 2q_{C,j}'' r_{j}\Delta r_{j}$$

where $q''_{t,j}$ is the heat flux on the top surface of the j-th control volume (or cell) of the transducer, and is given by either Eq. (6a) or Eq. (6c) depending on the location of the cell. The density, thermal conductivity, and specific heat capacity of the transducer are denoted by ρ_T , k_T and c_T , respectively, while z_T denotes its thickness. The radius of the j-th cell's center is denoted by r_j , while the radial span (grid size) is denoted by Δr_j . Eq. (7) is derived using the backward Euler time advancement method [17], wherein $T_{T,j}^{old}$ denotes the temperature of the j-th cell of the transducer at the previous time step. The heat flux through the bottom surface of the transducer or the interfacial contact (see Fig. 2) is denoted by $q''_{C,j}$, and is related to the contact conductance by the following relation:

$$q_{C,j}'' = G_C(T_{T,j} - T_{S,j,top}), (8)$$

where G_C is the contact conductance (in W/m²/K), and $T_{S,j,top}$ are the temperatures on the top surface of the substrate. Equation (8), in fact, serves to connect the transducer to the substrate, details of which will be discussed shortly. Substitution of Eq. (8) into Eq. (7), followed by rearrangement yields

$$\begin{bmatrix} \frac{k_{T}z_{T}(2r_{j} + \Delta r_{j})}{\Delta r_{j} + \Delta r_{j+1}} + \frac{k_{T}z_{T}(2r_{j} - \Delta r_{j})}{\Delta r_{j} + \Delta r_{j-1}} \\ + \rho_{T}c_{T}z_{T} \frac{2r_{j}\Delta r_{j}}{\Delta t} + 2G_{C}r_{j}\Delta r_{j} \end{bmatrix} T_{T,j}$$

$$- \left[\frac{k_{T}z_{T}(2r_{j} + \Delta r_{j})}{\Delta r_{j} + \Delta r_{j+1}} \right] T_{T,j+1} - \left[\frac{k_{T}z_{T}(2r_{j} - \Delta r_{j})}{\Delta r_{j} + \Delta r_{j-1}} \right] T_{T,j-1}$$

$$= \rho_{T}c_{T}z_{T} \frac{2r_{j}\Delta r_{j}}{\Delta t} T_{T,j}^{old} + 2q_{t,j}'' r_{j}\Delta r_{j} + 2G_{C}T_{S,j,top}r_{j}\Delta r_{j}$$
(9)

Equation (9) represents a set of N tri-diagonal equations that can be solved readily using the tridiagonal matrix algorithm [17].

In order to derive similar equations for the cells in the substrate, the finite-volume procedure is applied again, but now to the full two-dimensional equation, to yield

$$\begin{bmatrix}
\frac{k_{S}\Delta z_{k}(2r_{j}+\Delta r_{j})}{\Delta r_{j}+\Delta r_{j+1}} + \frac{k_{S}\Delta z_{k}(2r_{j}-\Delta r_{j})}{\Delta r_{j}+\Delta r_{j-1}} + \frac{4k_{S}r_{j}\Delta r_{j}}{\Delta z_{k}+\Delta z_{k+1}} \\
+ \frac{4k_{S}r_{j}\Delta r_{j}}{\Delta z_{k}+\Delta z_{k-1}} + \rho_{S}c_{S}\Delta z_{k}\frac{2r_{j}\Delta r_{j}}{\Delta t}
\end{bmatrix} T_{S,j,k}$$

$$-\left[\frac{k_{S}\Delta z_{k}(2r_{j}+\Delta r_{j})}{\Delta r_{j}+\Delta r_{j+1}}\right] T_{S,j+1,k} - \left[\frac{k_{S}\Delta z_{k}(2r_{j}-\Delta r_{j})}{\Delta r_{j}+\Delta r_{j-1}}\right] T_{S,j-1,k}$$

$$-\left[\frac{4k_{S}r_{j}\Delta r_{j}}{\Delta z_{k}+\Delta z_{k+1}}\right] T_{S,j,k+1} - \left[\frac{4k_{S}r_{j}\Delta r_{j}}{\Delta z_{k}+\Delta z_{k-1}}\right] T_{S,j,k-1}$$

$$= \rho_{S}c_{S}\Delta z_{k}\frac{2r_{j}\Delta r_{j}}{\Delta t} T_{S,j,k}^{old}$$
(10)

where thermal properties with subscript "S" denote those of the substrate. Similar equations may be derived for cells adjacent to the boundaries. These equations are not presented here for the sake of brevity. Equation (10), along with similar equations for the boundary cells, represent a system of five-banded linear algebraic equations that may be solved using any iterative solver tailored for banded systems. In this particular case, the Stone's strongly implicit method [17] is used.

Equations (9) and (10) are coupled, and are solved using the following iterative procedure:

- 1) The temperature on the top surface of the substrate, $T_{S,j,top}$, is first guessed. A reasonable guess may be the temperature of the ambient, *i.e.*, T_{∞} .
- 2) Equation (9) is then solved using a tridiagonal matrix algorithm. This yields the temperature of all cells of the transducer, namely $T_{T,j}$.
- Equation (8) is next used to compute the heat flux through the interface or contact.
- 4) The computed value of the flux serves as a boundary condition for the top surface of the substrate. With this boundary condition, Eq. (10), along with similar equations for the boundary cells in the substrate, are solved using the Stones's method.
- 5) Steps 1-4 are repeated until convergence.
- 6) Once convergence has been attained for the time step in question, the solution replaces the initial condition, and the procedure is repeated for the next time step.

Hyperbolic Heat Conduction Equation

The Fourier law can be derived from the BTE in the limit where the number of scattering events of the heat carriers, *i.e.*, phonons, is infinite. This limit may also be manifested by assuming an infinite group velocity of the phonons. The Fourier heat conduction equation does not contain any information pertaining to either the group velocity or the relaxation time-scale of the phonons. It is incapable of capturing any physical phenomena where the finite speed of the phonons may be of importance.

To overcome the aforementioned limitations of infinite wave speed as predicted by the Fourier heat conduction equation, a modification to Eq. (5) was proposed by Catteneo [8,9], in which, an additional transient term was introduced:

$$\rho c \tau \frac{\partial^2 T}{\partial t^2} + \rho c \frac{\partial T}{\partial t} = k \nabla^2 T = k \frac{\partial^2 T}{\partial z^2} + \frac{k}{r} \frac{\partial}{\partial r} \left(r \frac{\partial T}{\partial r} \right). \tag{11}$$

Equation (11) is a damped wave equation with wave speed $\sqrt{k/\rho c\tau}$, and is referred to as the *hyperbolic heat conduction equation*. This equation can also be derived from the BTE by taking its first moment [8,9]. It assumes that the time scales of interest are of the same order of magnitude as the relaxation time, whereas the length scales are much larger than the characteristic length scale for local thermodynamic equilibrium. This makes the hyperbolic heat conduction equation nonlocal in time but local in space. Therefore, the ballistic behavior of phonons is only partially captured by this model. In addition, the frequency dependent behavior of phonons cannot be modeled using this equation.

As far as discretization and the numerical solution of Eq. (11) is concerned, the procedure is very similar to the one described in the preceding section. The right hand side is discretized and spatial boundary conditions are applied in exactly the same manner as discussed earlier. The second derivative in time is discretized using the backward Euler method, as described elsewhere [17]. The numerical solution also follows the same algorithm outlined for the Fourier heat conduction equation. Once the temperature distribution has been computed, the heat fluxes are computed using

$$\tau \frac{\partial \mathbf{q}}{\partial t} + \mathbf{q} = -k \nabla T \tag{12}$$

rather than the Fourier law, *i.e.*, Eq. (12) is used instead of $\mathbf{q} = -k\nabla T$. One of the critical additional inputs to the hyperbolic heat conduction equation [Eq. (11)] is the effective relaxation time-scale of the phonons, τ . As to how it is determined is discussed in the next section.

RESULTS AND DISCUSSION

For the purposes of this study, the experimental data reported by Regner *et al.* [2] have been used for extraction of the thermal conductivity. The substrate in this experiment is a silicon block that is 525 μ m thick, *i.e.*, $z_s = 525 \mu$ m. The radial extent of substrate, r_s , is not known, and was assumed to be also equal to 525 μ m for the numerical calculations. The transducer is a bilayer transducer with 55 nm of gold and 5 nm of chromium, resulting in $z_T = 60$ nm. The thermophysical properties of silicon, gold and chromium that were used for calculations are shown in Table 1. Based on the thicknesses of the gold and

chromium layers, effective values of the properties of the transducer were estimated. These are also shown in Table 1.

Table 1: Thermophysical properties of the various materials used in the calculations.

		Transducer		
	Silicon	Gold	Chromium	Effective
Density (kg/m³)	2329	7140	19320	18290.8
Specific heat capacity (J/kg/K)	702	93.9	310	266.6
Thermal conductivity (W/m/K)	Calculated	450	129	155.7

For numerical calculations, a 200 x 200 nonuniform mesh with a stretching factor not exceeding 1.2 was used. This mesh was found to yield grid independent solutions. The modulation frequency, which is as an input parameter, was varied between 200 kHz and 200 MHz, and calculations were conducted for 22 different frequencies in this range. Each sinusoidal cycle of the laser was split into 5000 time steps. This implies that for high frequencies, a very small time-step size (~ 1 ps) was used to ascertain accurate temporal solutions. The nominal value of the interfacial (between the substrate and the transducer) contact conductance, G_C , was taken to be 200 MW/m²/K, as suggested by Cahill [1], although for a different material pair. A Gaussian profile was used for the laser heat flux with a $1/e^2$ radius of 3.5 um. The laser power was adjusted to attain a temperature rise of approximately 5 degrees at the center of the laser spot, as reported in the experimental description [2].

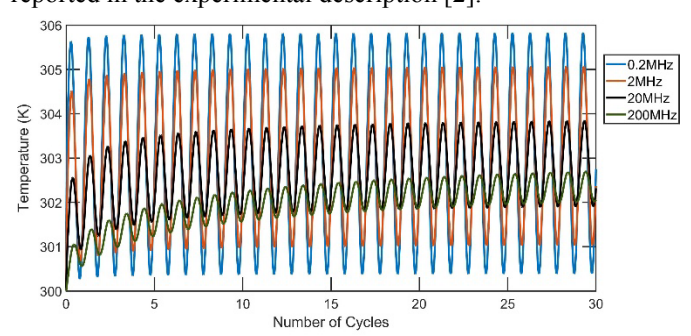


Figure 3: Computed temperature history at center of transducer for different frequencies.

For each modulation frequency, the calculations were advanced in time for several tens of cycles until the system exhibited quasi-steady behavior. The temperature-time history of the center of the transducer (origin in Fig. 1) was recorded. Figure 3 shows a plot of this data for 4 different frequencies. At low frequency, the transducer receives the laser flux for a longer period of time and, consequently, heats up more. This timedomain signal is post-processed to calculate the phase shift or lag between the pump laser and the computed temperature at the center of the transducer. The same calculation was repeated for several different thermal conductivity (of substrate) values. For each thermal conductivity value, a Phase Lag versus Frequency plot was generated. The error norms—both L1 norm and L2 norm—between the computed phase lag and the experimentally measured phase lag were then computed. The extracted (or desirable) thermal conductivity was chosen to be the one that minimized the error norm. In other words, it is a value that best fits the data over the entire range of frequency considered in this study. It was found that depending on which norm (L1 or L2) is used for best fit, the extracted value of thermal conductivity is slightly different, as discussed shortly.

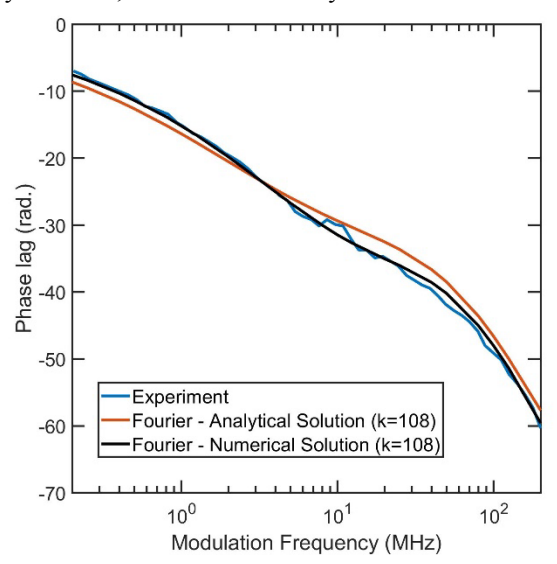


Figure 4: Phase lag calculated using the analytical and numerical models for k = 108 W/m/K.

For baseline numerical calculations, the top surface of the transducer outside of the laser spot was assumed to have heat loss with $h_t = 10 \text{ W/m}^2/\text{K}$. On the other hand, the far-field boundaries on the side and bottom were assumed to be isothermal at the ambient temperature ($T_{\infty} = 300$ K), which essentially corresponds to a very high heat transfer coefficient. Figure 4 shows a comparison of the phase lag obtained using the analytical and numerical solutions with experimental data reported by Regner et al. [2]. The curves shown represent the best fit to the experimental data using the L2 norm minimization criterion. For both the numerical model and the analytical model, the best fit is manifested by a thermal conductivity value of k =108 W/m/K. However, the fit is closer with the numerical model, as evident from the figure. If instead, the L1 norm minimization criterion is used, the best fit is obtained with a thermal conductivity value of 110 W/m/K. It is evident from Fig. 4 that in the case of the analytical model, the fit is not as good for intermediate and high frequencies as for low frequencies. To address this issue, previous researchers have suggested that, perhaps, one should consider a frequency-dependent thermal conductivity [5], while others have suggested using an anistropic thermal conductivity [18]. Yet others have tried to adjust the interface thermal conductance to obtain a better fit [11]. The fact that the numerical solution yields almost perfect fit at all frequencies, while the analytical model does not, suggests that this discrepancy maybe due to the assumptions invoked in the derivation of the analytical solution rather than absence of necessary physics in the model. These include semi-infinite media (in the radial direction), the contact surface being treated as a volume and has lateral conduction, lack of heat loss from the top of the system, among others.

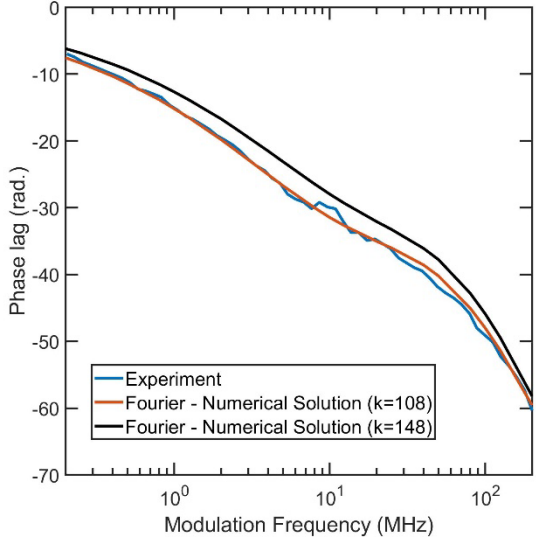
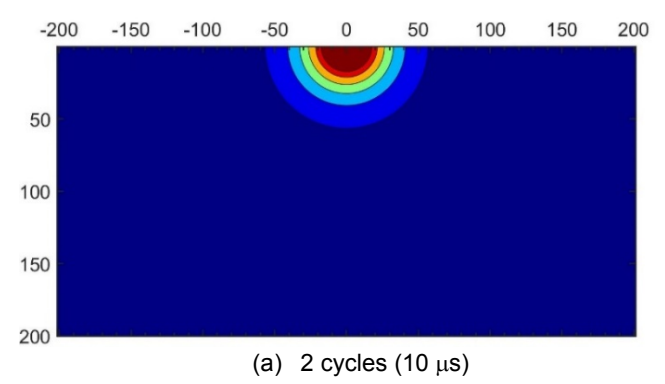


Figure 5: Phase lag computed using the numerical model with two different thermal conductivity values.

The extracted value of thermal conductivity, namely k=108 W/m/K is significantly smaller than the bulk thermal conductivity of silicon at 300K, which is about 148 W/m/K. This reduction in thermal conductivity represents the so-called *thermal conductivity suppression* reported in the literature [6,7]. The phase lag versus frequency behavior with the bulk value of thermal conductivity is shown in Fig. 5. The phase lag is slightly underpredicted at all frequencies if the bulk value of thermal conductivity is used. For the same experimental data set, Regner *et al.* [2] reported a thermal conductivity of 99 \pm 6 W/m/K.

The spatiotemporal evolution of the nondimensional temperature distribution and the heat wave is illustrated in Fig. 6 for a modulation frequency of 200 kHz. For clarity of visualization only a small portion of the substrate is shown. Since the penetration depth of the heat wave is inversely proportional to the inverse square root of the modulation frequency, and 200 kHz is the smallest frequency considered in this study, the distributions shown in Fig. 6 represent the highest penetration of the heat wave among all cases considered. After 30 cycles, the system has almost reached quasi-steady state. Since the substrate (and computational domain) is of size 525 µm in both directions, and the heat wave has not even penetrated 200 µm in the worstcase scenario, it is fair to conclude that the computational domain is large enough for the far-field boundary conditions at the top and side to have minimal effect on the results. This is corroborated next using additional calculations.



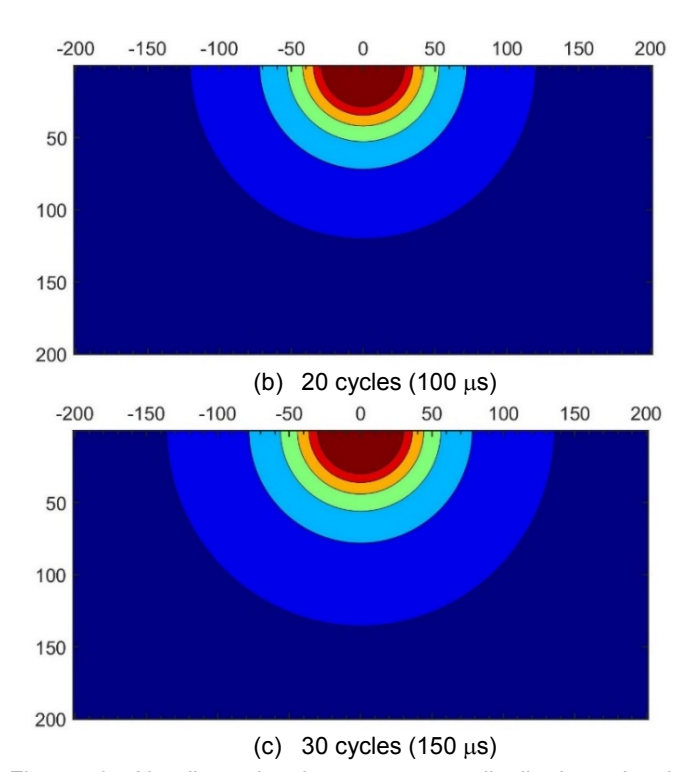


Figure 6: Nondimensional temperature distributions in the substrate after various intervals of time.

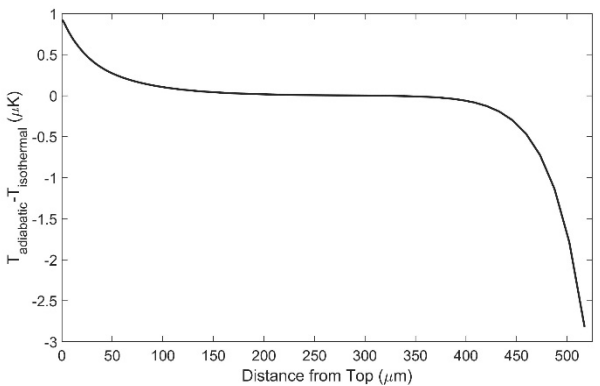


Figure 7: Computed temperature difference along the centerline of the substrate between adiabatic and isothermal boundary condition at the bottom surface at quasi-steady state.

As mentioned earlier, the baseline calculations (reported above) were conducted using isothermal boundary conditions at the bottom and side boundaries. An isothermal boundary with T_{∞} corresponds to h_s , $h_b \to \infty$. To investigate the sensitivity of this boundary condition on the computed results, the solution was recomputed with an adiabatic boundary condition instead of an isothermal boundary condition. An adiabatic boundary condition represents the other extreme wherein the heat transfer coefficients are zero. Figure 7 shows the difference in the temperature along the centerline (axis) of the substrate. Clearly, there is no meaningful difference implying that the boundary condition has no impact on the results. This may be attributed to the fact that the computational domain is much larger than the penetration depth. Likewise, the heat transfer coefficient on the top of the transducer was changed from 10 W/m²/K to 250

 $W/m^2/K$, and the maximum change in temperature anywhere on the transducer was found to be 5.5 μ K.

One of the critical inputs to the model considered here is the interface conductance, G_c . For the baseline calculations, a value of 200 MW/m²/K was used, in accordance with Cahill [1]. Other researchers have suggested a value in the range 160-250 MW/m²/K [11]. To understand the sensitivity of the extracted thermal conductivity to this unknown parameter, computations were performed for various values of $G_{\mathcal{C}}$. Figure 8 shows the predicted phase lag for various values of G_c and a thermal conductivity of 108 W/m/K. There is clearly some difference in the results at intermediate and high modulation frequencies. If $G_C = 250 \text{ MW/m}^2/\text{K}$ is used as the interface conductance, the best fit to the experimental data is obtained with a thermal conductivity value of 115 W/m/K, rather than 108 W/m/K. On the other hand, for the other two values considered, the best fit yields 108 W/m/K, although the quality of the fit is better for G_C = 200 MW/m²/K than for G_C = 160 MW/m²/K.

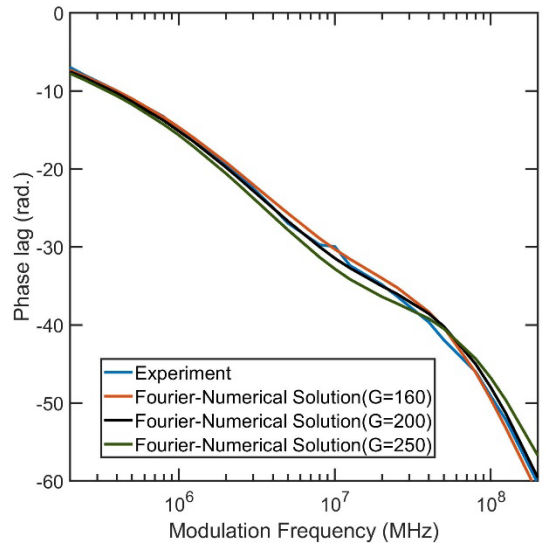


Figure 8: Effect of interface conductance on the phase lag.

Finally, all calculations were repeated using the hyperbolic heat conduction equation. The effective (or average) relaxation time-scale, τ , which appears as an input in the hyperbolic heat conduction equation was estimated using the following relationship [19]:

$$\tau = \frac{\sum_{p} \int_{\omega_{\min,p}}^{\omega_{\max,p}} c_{\omega,p} \left| \mathbf{v}_{\omega,p} \right|^{2} \tau_{\omega,p} d\omega}{\sum_{p} \int_{\omega_{\min,p}}^{\omega_{\max,p}} c_{\omega,p} \left| \mathbf{v}_{\omega,p} \right|^{2} d\omega},$$
(13)

where $c_{\omega,p}$ is the spectral specific heat capacity of silicon, and and $\mathbf{v}_{\omega,p}$ is the spectral group velocity of the phonons. Both of these quantities can be computed directly for any polarization p and frequency ω using dispersion relationships of silicon, as explained elsewhere [8,20]. The value of the effective relaxation time-scale using Eq. (13) and frequency and polarization dependent time-scale expressions proposed by Holland [21,22]

was found to be about 0.0365 ns. The largest difference in temperature as predicted by the two models (Fourier versus Hyperbolic) is manifested at the highest modulation frequency (200 MHz) and it occurs on the surface of the substrate, as shown Fig. 9. This is understandable since at high frequency, quasiballistic effects are expected to be the strongest and consequently, some difference is expected between the two models. However, even for 200 MHz, the cycle time is 5 ns, which is significantly larger than the estimated effective relaxation time scale. This implies that the hyperbolic heat conduction equation is expected to behave similar to the Fourier heat conduction equation in this particular case, as is evident from the fact that 0.05 K (out of about 2.1 K rise) was the largest temperature difference observed between the two models. The phase lag calculated using the two models was found to be identical, and therefore, the resulting thermal conductivity did not change. Again, this is to be expected since the relaxation time-scale used in the calculations is significantly smaller than the cycle time for any modulation frequency considered. The choice of the effective relaxation time-scale requires further investigation.

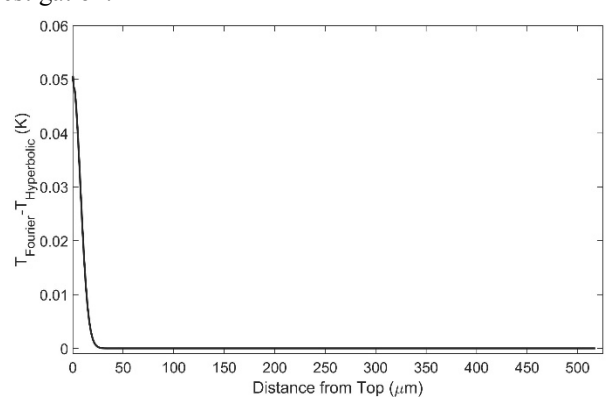


Figure 9: Computed temperature difference along the centerline of the substrate between the Fourier heat conduction and Hyperbolic heat conduction equations with a modulation frequency of 200 MHz and after 30 cycles.

SUMMARY AND CONCLUSIONS

Calculations were conducted both analytically and numerically to extract the thermal conductivity of a silicon substrate from FDTR experimental data. The analytical calculations used Hankel transforms of the Fourier heat conduction equation in frequency domain along with the Feldman algorithm to treat multiple finite-sized layers. The numerical calculations were conducted in time domain using the finite-volume method and a backward Euler time advancement scheme. Both the Fourier heat conduction equation and the hyperbolic heat conduction equation were explored for numerical solutions. The numerical solutions enable use of more realistic boundary conditions, namely convective heat loss at the surfaces of the substrate and transducer. The calculations were conducted in the range of modulation frequency going from 200 kHz to 200 MHz for 22 different frequencies. The phase lag between the modulated pump laser signal and the temperature of the transducer at the center of the laser beam was calculated in each case and a plot of phase lag versus frequency was generated. This plot was

compared to the same plot measured experimentally, and the thermal conductivity was adjusted to obtain the best fit. The extracted thermal conductivity was found to be in the range 108-115 W/m/K depending on the choice of boundary conditions and the interface conductance between the transducer and the substrate used in the calculations. This value is slightly different from the value of 99 ± 6 W/m/K reported earlier for the same experimental dataset. Parametric studies revealed that the extracted thermal conductivity is more sensitive to the interface thermal conductance than the boundary conditions at the surfaces of the substrate/transducer. For this particular case, the hyperbolic heat conduction equation yielded identical results as the Fourier heat conduction equation.

ACKNOWLEDGMENTS

The Ohio Supercomputer Center (OSC) and the Department of Mechanical and Aerospace Engineering at the Ohio State University are gratefully acknowledged for providing computational resources.

REFERENCES

- [1] Cahill, D. G., (2004), "Analysis of heat flow in layered structures for time domain thermo-reflectance," *Review of Scientific Instruments*, **75**, p. 5119.
- [2] Regner, K.T., Sellan, D.P., Su, Z., Amon, C.H., McGaughey, A.J.H., Malen, J.A., (2013), "Broadband phonon mean free path contributions to thermal conductivity to thermal conductivity measured using frequency domain themroreflectance" *Nature Communications*, 4: p. 1640
- [3] Minnich, A.J., Johnson, J.A., Schmidt, A.J., Esfarjani, K., Dresselhaus, M.S., Nelson, K.A., and Chen, G., (2011), "Thermal Conductivity Spectroscopy Technique to Measure Phonon Mean Free Paths," *Physical Review Letters*, **107**, p. 095901
- [4] Feldman, A., (1999), "Algorithm for solutions of the thermal diffusion equation in a stratified medium with a modulated heating source", *High Temperatures High Pressures*, **31**, pp. 293-298.
- [5] Koh, Y.K., and Cahill, D.G., (2007), "Frequency Dependence of the Thermal Conductivity of Semiconductor Alloys," *Physical Review B*, **76**, pp. 075207.
- [6] Minnich, A.J., (2012), "Determining Phonon Mean Free Paths from Observations of Quasiballistic Thermal Transport," *Physical Review Letters*, **109**, p. 205901.
- [7] Hua, C., and Minnich, A.J., (2014), "Transport Regimes in Quasiballistic Heat Conduction," *Physical Review B*, **89**, p. 094302.
- [8] Tien, C.L., Majumdar, A., and Gerner, F.M., eds., 1998, *Microscale Energy Transport*, Taylor and Francis.
- [9] Zhang, Z., (2007), Nano/Microscale Heat Transfer, McGraw Hill, New York.
- [10] Ramu, A.T. and Bowers, J.E., (2015), "A compact heat transfer model based on an enhanced Fourier law for

- analysis of frequency domain thermoreflectance experiments," *Applied Physics Letters*, **106**, p. 263102.
- [11] Ma, Y., (2014), "A two-parameter nondiffusive heat conduction model for data analysis in pump-probe experiments," *Journal of Applied Physics* **116**, p. 243505.
- [12] Chen, G., (2001), "Ballistic-Diffusive Heat-Conduction Equations," *Physical Review Letters*, **86**(11), pp. 2297–2300.
- [13] Mittal, A., and Mazumder, S., (2011), "Generalized Ballistic-Diffusive Formulation and Hybrid S_N-P_N Solution of the Boltzmann Transport Equation for Phonons for Non-Equilibrium Heat Conduction," *Journal of Heat Transfer*, **133**(9), p. 092402.
- [14] Mittal, A., and Mazumder, S., (2011), "Hybrid Discrete Ordinates—Spherical Harmonics Solution to the Boltzmann Transport Equation for Phonons for Non-Equilibrium Heat Conduction," *Journal of Computational Physics*, **230**(18), pp. 6977-7001.
- [15] Ali, S.A. and Mazumder, S., (2017), "Phonon Boltzmann Transport Equation Based Modeling of Time Domain Thermo-Reflectance Experiments," *International Journal of Heat and Mass Transfer*, **107**, pp. 607-621.
- [16] Carslaw, H.S. and Jaeger, J.C., (1959), *Conduction of Heat in Solids*, Second edition, Oxford University Press.
- [17] Mazumder, S., (2016), Numerical Methods for Partial Differential Equations: Finite Difference and Finite Volume Methods, First Edition, Academic Press, New York.
- [18] Feser, J.P. and Cahill, D.G., (2012), "Probing anisotropic heat transport using time-domain thermoreflectance." *Review of Scientific Instruments*, **83**, p. 104901.
- [19] Allu, P. and Mazumder, S., (2018), "Comparative assessment of deterministic approaches to modeling quasiballistic phonon heat conduction in multi-dimensional geometry," *International Journal of Thermal Sciences*, **127**, pp. 181-193.
- [20] Mazumder, S., and Majumdar, A., (2001), "Monte Carlo Study of Phonon Transport in Solid Thin Films Including Dispersion and Polarization," *Journal of Heat Transfer*, **123**, pp. 749-759.
- [21] Holland, M.G., (1963), "Analysis of lattice thermal conductivity," *Physical Review*, **132**(6), pp. 2461-2471.
- [22] Holland, M.G., (1964), "Phonon scattering in semiconductors from thermal conductivity studies," *Physical Review*, **134**(2A), pp. A471-A480.